Chemical Science

EDGE ARTICLE

Atomically-thin non-layered cobalt oxide porous sheets for highly efficient oxygen-evolving electrocatalysts†

Yongfu Sun,‡ Shan Gao,‡ Fengcai Lei, Jiawei Liu, Liang Liang and Yi Xie*

Water electrolysis for hydrogen production requires better catalysts to lower the kinetic barrier of the oxygen evolution reaction. Herein, conceptually-new, noble-metal-free, porous, atomically-thick sheets are first put forward as an excellent platform to promote the oxygen evolution activity through affording abundant catalytically active sites and enhanced two-dimensional conductivity. As an example, the synthetic porous Co_3O_4 atomically-thick sheets with a thickness of 0.43 nm and about 30% pore occupancy afford low-coordinated Co^{3+} atoms to serve as the catalytically active sites, while the obviously increased density of states at the valence band and conduction band edge facilitate fast electron transport along their two-dimensional conducting paths. As a result, the porous, atomically-thick Co_3O_4 sheets exhibit an electrocatalytic current up to 341.7 mA cm^{-2}, roughly 50-times larger than that of the bulk counterpart and even more strikingly higher than that of most existing reports under similar conditions. This work holds great promise for triggering breakthroughs in the field of electrocatalysis.

Introduction

Solar hydrogen production from abundant sources such as water and CO_2 could offer a clean and sustainable pathway to ameliorate stringent global energy demands and environmental sustainability.[1] Up to now, a variety of approaches including photochemical, photoelectrochemical and solar thermochemical methods have been developed to produce clean and renewable hydrogen fuel through utilizing the free and unlimited supply of solar energy.[2] However, the overall efficiency of the above solar hydrogen production methods is largely limited by the kinetically sluggish oxygen evolution reaction (OER), which proceeds through a complex four-electron redox process and usually requires a high overpotential.[3] Although previous studies have shown that some noble metals and their oxides, such as Ru, Ir, RuO_2, IrO_2, could efficiently catalyze the OER process,[4] their low abundance and high cost impede their commercial utilization. Recently, many earth-abundant metal oxides have been intensely researched as potential OER catalysts to replace the expensive Ru- and Ir-based compounds.[5] Among these catalytic materials, spinel Co_3O_4 has emerged as a promising candidate for investigating the water oxidation

reaction *via* photocatalytic and electrocatalytic processes,[2a,6] thanks to their environmental friendliness, abundance of reserves, thermal stability and low cost of raw materials. However, compared to the precious metals-based OER catalysts, Co_3O_4 still exhibits a relatively low catalytic activity, which has unfortunately limited its large-scale applications. This is mainly ascribed to the inherently poor electrical conductivity of Co_3O_4[7] and the extremely low amount of active sites in the previously prepared Co_3O_4 catalysts. Of note, despite recent studies having demonstrated that a few amorphous metal oxides with disordered structures could show excellent OER activities,[8] the limited fabrication methods and the difficulties in their characterization impede their wide extension to many other metal oxides. Thus, it is highly desirable and imperative to fabricate a novel crystalline material with abundant active sites and increased conductivity as well as disordered atomic structures, with efforts to achieve a highly efficient OER catalytic activity.

Herein, conceptually-new, noble-metal-free, porous, atomically-thick sheets are put forward as an excellent platform to promote oxygen evolution activity through affording abundant catalytically active sites and increased two-dimensional (2D) conductivity. The ultrathin atomic thickness could offer an extremely large fraction of coordinated-unsaturated surface atoms, which could serve as the active sites to expedite the oxygen evolution reaction. Meanwhile, the ultra-large specific surface area allows oxygen evolution reactions to take place across a much bigger area, greatly enlarging the reaction space.[1a,9] In addition, previous studies have demonstrated that the atomically-thick sheets usually possess obvious structure

Hefei National Laboratory for Physical Sciences at Microscale, Collaborative Innovation Center of Chemistry for Energy Materials, University of Science & Technology of China, Hefei, Anhui 230026, P.R. China. E-mail: yxie@ustc.edu.cn; Fax: +86-551-63606266

† Electronic supplementary information (ESI) available: Supplementary crystal structure, formation mechanism and figures. See DOI: 10.1039/c4sc00565a

‡ These authors contributed equally to this work.

disorder on their surface,[1a,9,10] which always leads to a remarkably increased density of states (DOS) near the Fermi level. This facilitates fast electron transport along the 2D conducting channels and hence accelerates the sluggish OER kinetics. More importantly, the presence of abundant pores in the atomically-thick sheets could not only provide more active atoms with lower coordination number, but also allow for easy electrolyte infiltration to the inside of the catalysts, which contribute to offering more active sites to involve the following physico-chemical reactions and hence achieve an improved energy conversion efficiency.

Inspired by the aforementioned concepts, the controllable synthesis of porous Co_3O_4 atomically-thick sheets is of vital importance and practical significance. To date, it is well-known that atomically-thick sheets for layered compounds could be easily fabricated through controllable exfoliation of their corresponding anisotropic layered bulk materials.[1a,10,11] However, for non-layered compounds, especially for cubic Co_3O_4 without anisotropy, the controllable synthesis of their atomically-thick sheets is extremely challenging on account of the hard breakage of their strong in-plane bonds and the lack of intrinsic driving force for 2D anisotropic growth,[9,12] let alone the synthesis of their porous atomically-thick sheets. It is noticeable that the typical strategies for fabricating porous materials usually contain the template-directed method and the chemical etching process.[13] In spite of the fact that these traditional strategies could be utilized to fabricate porous materials in bulk or film structure forms, they are unable to produce porous ultrathin sheets, especially porous atomically-thick sheets with a thickness of less than 1 nm. Accordingly, it is essential and challenging to pursue new approaches for generating porous, atomically-thick sheets.

Results and discussion

Herein, a convenient and scalable fast-heating strategy was developed for synthesizing clean and freestanding, noble-metal-free, porous, atomically-thick sheets with non-layered structures, taking the cubic Co_3O_4 as an example (Fig. S1†). Fig. S2A† illustrates that the successful synthesis of clean, porous, atomically-thick Co_3O_4 sheets benefits from an intermediate precursor of atomically-thick CoO sheets (Fig. S2–S5†). From our systematic study, we observed that CoO initially nucleated at 190 °C accompanied by the partial oxidation of $HOCH_2$-CH_2OH into $HOCH_2COOH$, which was verified by the corresponding FTIR spectrum in Fig. S5A.† Simultaneously, $HOCH_2COO^-$ could be adsorbed on the surface of the CoO nuclei to reduce their surface energy (Fig. S2A and S2B†), while the presence of $HOCH_2COO^-$ conferred a net negative charge to the CoO nuclei due to ionization of the carboxyl groups. In addition, van der Waals interactions and hydrogen bonds between the $HOCH_2COO^-$ caused directional short-range attractions between the CoO nuclei. In this case, driven by the electrostatic interactions and directional short-range attractions,[14] the CoO nuclei self-assembled into atomically-thin two-dimensional CoO sheets with an average thickness of *ca.* 0.44 nm (Fig. S2C and S2D, S3 and S4†). And then, upon heating at

400 °C for a very short time of 5 min in air, the cubic CoO transformed into cubic Co_3O_4 (Fig. S2 and S6†), while the quick combustion/decomposition of $HOCH_2COO^-$ resulted in the formation of numerous pores on the surface of the as-obtained Co_3O_4 sheets (Fig. S2A, S5B and S7†). Notably, the developed fast-heating strategy is convenient, high-yield and can be easily scaled up for the large-scale synthesis of porous, atomically-thick, non-layered materials.

The above obtained Co_3O_4 powders were collected for further detailed characterizations. Of note, XRD measurement was carried out on the collected powder sample accumulated by the as-obtained ultrathin sheets by reason that it was not possible to perform XRD characterization on an individual ultrathin sheet. The corresponding XRD peaks in Fig. S6A† could be readily indexed to the spinel phase of Co_3O_4 with a cubic structure, corresponding to JCPDS no. 78-1969. In addition, their XPS spectra in Fig. S6B–D† showed that the obtained products consisted of elements Co and O, while no evident impurities were detected, which demonstrated the formation of pure Co_3O_4,[15] further confirmed by the corresponding IR spectrum in Fig. S5A.† Inductively coupled plasma atomic emission spectrometry shows that the Co/O molar ratio is about 0.755, fairly consistent with the stoichiometry of Co_3O_4, further verifying that the finally obtained products were pure Co_3O_4. Their Raman modes showed broadening and obviously shifted towards a lower wavenumber side compared with the Raman modes of bulk Co_3O_4 (Fig. 1C), which was mainly ascribed to the phonon confinement effect and indicated the ultrathin thickness.[1a,16] As shown by the TEM images in Fig. 1A and 1B and in Fig. S7,† the nearly transparent feature suggested the ultrathin thickness of the as-obtained Co_3O_4 sheets, further verified by their AFM measurements in Fig. 1E and 1F. More importantly, the TEM images in Fig. 1A and 1B, S7† and the HRTEM image in Fig. 1D clearly demonstrated the presence of abundant pores on the surface of the ultrathin Co_3O_4 sheets, in which the pores possessed an occupancy of about 30%, which was further verified by the AFM image and sharp peaks in the corresponding
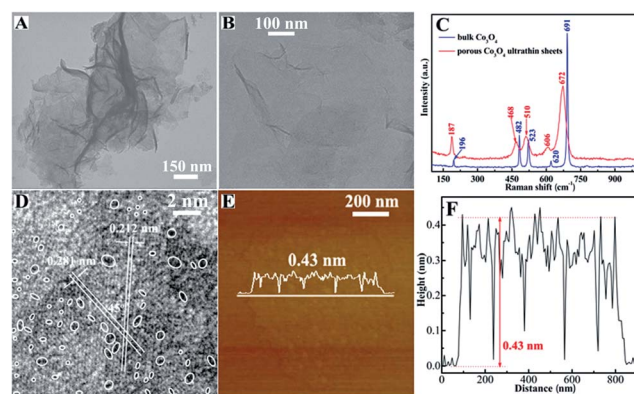
Fig. 1 (A,B) TEM images, (D) HRTEM image, (E) AFM image and (F) the height profile along the white line indicated in (E) for porous Co_3O_4 atomically-thin sheets; the inset circles in (D) denote the presence of pores on their surface. (C) Raman spectra for porous Co_3O_4 ultrathin sheets and the bulk counterpart.

height profile (Fig. 1E and 1F). Also, the HRTEM image in Fig. 1D depicted that the ultrathin Co_3O_4 sheets possessed a [001] orientation, while their AFM image and the corresponding height profile in Fig. 1E and 1F showed a uniform thickness of 0.43 nm, corresponding to the thickness of half a unit cell along the [001] direction (Fig. S1†). Therefore, all of the above results illustrated the formation of clean, porous, atomically-thin Co_3O_4 sheets with a thickness of half a unit cell.

Thanks to their ultrathin thickness of 0.43 nm and the 30% pore occupancy, the porous Co_3O_4 atomically-thin sheets possessed an extremely large surface area of 152.1 m^2 g^{-1} and an ultrahigh fraction of coordination-unsaturated surface atoms, which reasonably contributed to promoting greatly the electrochemical oxidation of water to oxygen. To study the electrocatalytic activity of the porous Co_3O_4 atomically-thin sheets, they were prepared on a glassy carbon (GC) electrode for electrocatalyzing oxygen evolution in 1.0 M KOH. In effect, Fig. 2A depicts the linear sweeps in an anodic direction for the modified electrodes consisting of porous Co_3O_4 atomically-thin sheets, bulk Co_3O_4 and commercial 20 wt% Pt/C, respectively.

As expected, the bare GC electrode was totally inactive towards O_2 production. By contrast, the porous Co_3O_4 atomically-thin sheets exhibited significantly improved current densities in comparison with the bulk counterpart and the commercial 20 wt% Pt/C. For example, the porous Co_3O_4 atomically-thin sheets possessed an electrocatalytic current density up to 341.7 mA cm^{-2} at 1.0 V vs. Ag/AgCl, roughly 50- and 30-times larger than that of the bulk counterpart and the commercial 20 wt% Pt/C (Fig. 2A), strongly highlighting their fascinating superiority in promoting the oxygen evolution activity. Actually, such an electrocatalytic reaction current of 341.7 mA cm^{-2} was much better than that of most existing reports under similar conditions (Fig. 2E),[3,17] indicating the highly efficient electron transport in the porous Co_3O_4 atomically-thin sheets. This could be attributed to their extremely large fraction of coordination-unsaturated surface atoms, which could serve as the active sites to accelerate the OER process. Moreover, as depicted in Fig. 2B, one can clearly observe that the Tafel plot of the porous Co_3O_4 atomically-thin sheets displayed a linear dependence of the logarithm of current density, whereas the corresponding Tafel slope was down to ca. 25 mV per decade, much smaller than that of the bulk counterpart, commercial 20 wt% Pt/C and other reported Co-based OER catalysts (Fig. 2E).[6b,17a,c] It is noticeable that the smaller Tafel slope is more beneficial for practical applications, since it can provide a remarkably increased OER rate with the increase of overpotentials. Furthermore, besides the catalytic activity, it is well-established that the material's stability is also a crucial factor in developing cost-effective catalysts for water splitting. To evaluate the stability in a basic environment, the long-term cycling stability of the Co_3O_4 samples was investigated by performing continuous cyclic voltammetry (CV) between 0 and 1.0 V vs. Ag/AgCl at 50 mV s^{-1}. In fact, the stability tests showed that the porous Co_3O_4 atomically-thin sheets were inherently stable during the OER cycling. As shown in Fig. 2C, even after 10 000 CV cycles, the porous Co_3O_4 atomically-thin sheets still afforded almost the same j–V curve as the initial cycle, whereas the bulk counterpart showed a 76.2% drop in the anodic current density, clearly revealing the former's superior structural stability in alkaline solutions.

Of note, the greatly improved electrocatalytic oxygen evolution properties of the porous Co_3O_4 atomically-thin sheets could be ascribed to the synergistic effect between their macroscopic morphological features and their microscopic atomic/electronic structure. It is noticeable that the Co^{3+} atoms in Co_3O_4 have been well regarded as the catalytically active sites for electrocatalytic water oxidation.[18] As is well-known, the Co^{3+} atom has a percentage as high as 66.7% in the overall Co atoms of Co_3O_4, while the interior and surface Co^{3+} atoms of Co_3O_4 have a coordination number of 6 and 5, respectively (Scheme 1B). Notably, for the synthetic porous Co_3O_4 atomically-thin sheets, the presence of pores could decrease the coordination number of Co^{3+} atoms to 4 or even 3 (Scheme 1B), while the ultrathin thickness of half a unit cell enables them to expose all Co^{3+} atoms on their surfaces, indicating that all the Co^{3+} atoms could serve as the active sites to catalyze the water oxidation reactions. It is well-documented that H_2O molecules are initially adsorbed on the surface of catalysts during the water oxidation

Catalyst	Current density (mA cm^{-2})	Tafel slope (mV/dec)	Potential (V vs. RHE)	Catalyst loading (mg cm^{-2})	Electrolyte
N-doped C[3a]	54.5	--	1.8	0.2	0.1 M KOH
Mn_3O_4/$CoSe_2$[3b]	16.5	49	1.75	0.2	0.1 M KOH
Co_3O_4/N-rmGO[17a]	72	67	1.6	1	1 M KOH
Co_3O_4/Ni foam[17c]	150	47	2.02	1	1 M KOH
Co_3O_4[17d]	126.9	--	2.02	0.13	1 M KOH
Ni foam[17e]	160	--	2.02	--	1 M KOH
Co_3O_4[i]	341.7	25	2.02	0.34	1 M KOH
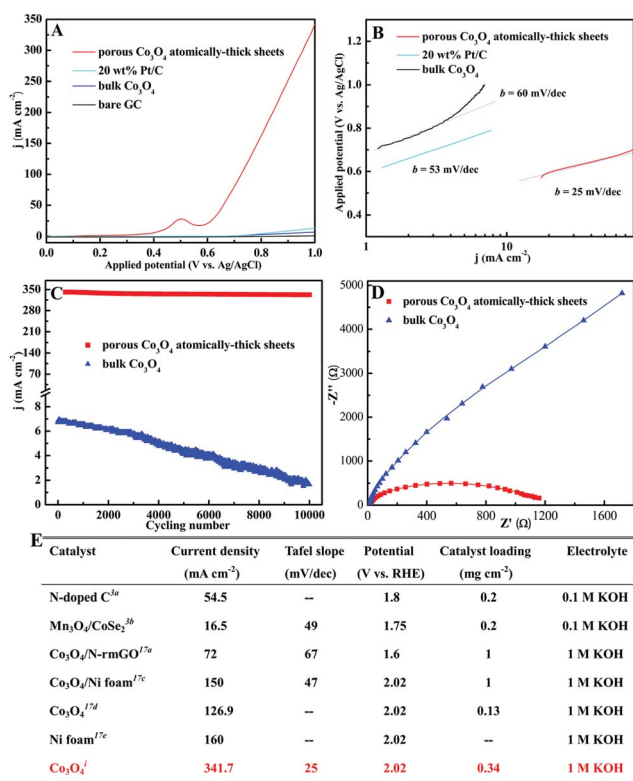
Fig. 2 (A) Polarization curves for the OER on a bare GC electrode, porous Co_3O_4 atomically-thin sheets, bulk Co_3O_4 and commercial 20 wt% Pt/C, respectively; sweep rate: 5 mV s^{-1}. (B) Tafel plot (overpotential versus log current) derived from (A). (C) Durability test showing negligible current loss even after 2000 CV cycles at a scan rate of 50 mV s^{-1}. (D) Electrochemical impedance spectra at 1.0 V vs. Ag/AgCl for the electrodes consisting of porous Co_3O_4 atomically-thin sheets and bulk Co_3O_4; Z' and Z'' were the real and imaginary parts of impedance, respectively. (E) Electrocatalytic water oxidation properties for other reported products: rmGO stands for reduced mildly oxidized graphene oxide; 'i' refers to this work.
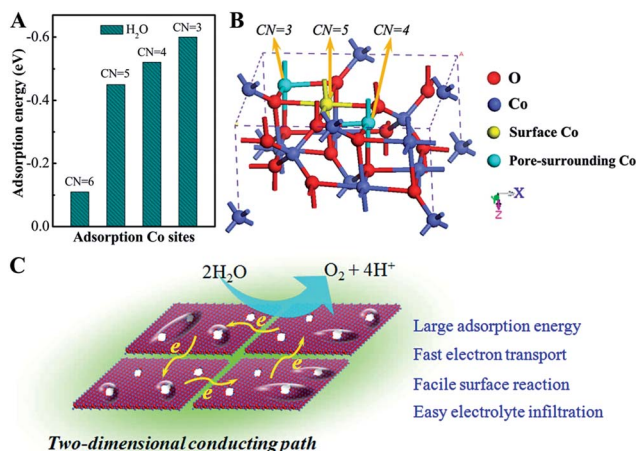
Scheme 1 (A) Calculated adsorption energy for H_2O molecules on Co^{3+} sites with different coordination number (CN). (B) Crystal structure shows the different coordination numbers for surface and pore-surrounding Co^{3+} atoms. (C) Advantages of using the porous Co_3O_4 atomically-thin sheets for electrocatalytic water oxidation.

reaction and hence the following reactions proceed (* denotes the active sites):[19]

$$2H_2O + * \rightarrow OH^* + H_2O + e^- + H^+ \quad (1)$$

$$OH^* + H_2O \rightarrow O^* + H_2O + e^- + H^+ \quad (2)$$

$$O^* + H_2O \rightarrow OOH^* + e^- + H^+ \quad (3)$$

$$OOH^* \rightarrow O_2 + e^- + H^+ \quad (4)$$
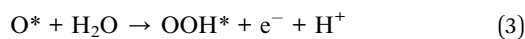
That is to say, the adsorption energy of the H_2O molecules plays a crucial role in affecting the OER activity. Note that the water oxidation reactions usually occur on the surface of the catalyst on account of their lower coordination number and higher catalytic activity, further confirmed by density-functional-theory (DFT) calculations. As shown in Scheme 1A, DFT calculations revealed that the 5-coordinated surface Co^{3+} atoms possessed an adsorption energy (absolute value) of 0.45 eV, obviously larger than that of 6-coordinated interior Co^{3+} atoms, indicating that the low-coordinated surface Co^{3+} atoms were more favorable for adsorbing H_2O molecules (Scheme 1C). In addition, Scheme 1A also illustrated that the adsorption energy of H_2O molecules on Co^{3+} atoms gradually increased with their coordination number decreasing from 5 to 3, suggesting that the lower coordination number usually led to a higher catalytic activity. Moreover, the 2-coordinated surface Co^{2+} atoms possessed a calculated adsorption energy of 0.18 eV, much smaller than that of the 5-coordinated surface Co^{3+} atoms, further demonstrating that the Co^{3+} atoms are the most active sites for electrocatalytic water oxidation. In our synthetic porous Co_3O_4 atomically-thin sheets, the ultrathin thickness of 0.43 nm nearly realized the ultimate upper limit of specific surface area, which enabled the generation of 5-coordinated Co^{3+} atoms on their surfaces; meanwhile, the 30% pore occupancy further helped to create coordinately unsaturated Co^{3+} atoms with a

coordination number lower than 5. All the low-coordinated Co^{3+} atoms could serve as the catalytically active sites to maximize the H_2O adsorption and hence are effectively involved the following water oxidation reactions. Also, the presence of numerous pores facilitated easy electrolyte infiltration into the interior atomically-thin Co_3O_4 sheets and hence ensured good electrical contact with the electrolyte, thus greatly improving their surface reactions.[20] Moreover, the 2D configuration with its extremely large surface area provided intimate contact with the GC electrode and a high interfacial contact area with the electrolyte, thus guaranteeing fast interfacial charge transfer and facile electrochemical reactions as well as low corrosion rates.[1a,9,16a] This could be further verified by the much lower interfacial charge-transfer resistance for the porous Co_3O_4 atomically-thin sheets (Fig. 2D), which enabled their electron transport and cycling stability to be greatly enhanced during the electrocatalytic process. Furthermore, it was well-established that the ultrathin 2D sheets usually possessed obvious structural disorder,[1a,9,16a] which always resulted in an apparently increased density of states at the edge of the valence band or conduction band and hence led to fast electron transport. As
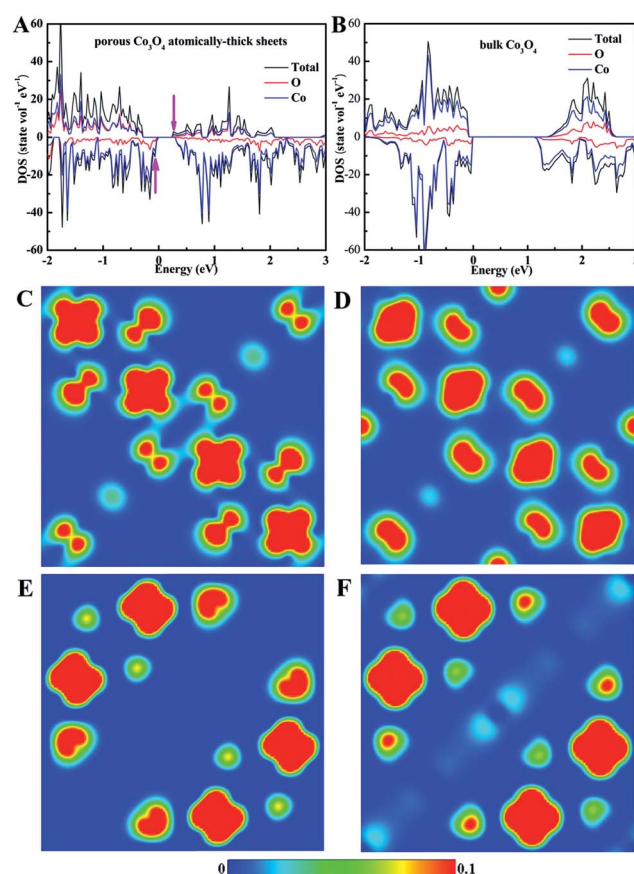
Fig. 3 (A,B) Calculated DOS for the porous Co_3O_4 atomically-thin sheets and bulk counterpart; insets clearly depict the increased DOS at the valence band and conduction band edge of the porous Co_3O_4 atomically-thin sheets. Charge density wave along the (001) plane for the valence band and conduction band edge of (C,E) porous Co_3O_4 atomically-thin sheets and (D,F) bulk counterpart, respectively.

expected, Fig. 3A and 3B reveal that the porous Co_3O_4 atomically-thin sheets displayed a significantly increased DOS at the edge of the valence band and conduction band with respect to their bulk counterpart, which was further verified by their calculated charge density wave at the valence band edge in Fig. 3C and 3D and at the conduction band edge in Fig. 3E and 3F. In this case, the two-dimensional conducting paths allowed for much faster electron transport in the porous Co_3O_4 atomically-thin sheets, which was further confirmed by their obviously smaller charge-transfer resistance in Fig. 2D, thus definitely determining their remarkably enhanced oxygen evolution activity.

Conclusions

In conclusion, conceptually-new, noble-metal-free, porous, atomically-thin sheets were proposed as an excellent platform to promote OER activity through affording abundant catalytically active sites and enhanced two-dimensional conductivity. As an example, porous Co_3O_4 atomically-thick sheets with a thickness of half a unit cell along with a *ca.* 30% pore occupancy were first successfully synthesized *via* a convenient and scalable fast-heating strategy, taking advantage of an intermediate precursor of atomically-thick CoO sheets. The ultrathin thickness of 0.43 nm afforded 5-coordinated Co^{3+} atoms and 4-/3-coordinated pore-surrounding Co^{3+} atoms to serve as the catalytically-active sites, while the obviously increased DOS at the valence band and conduction band edge allowed for rapid electron transport along the two-dimensional conducting paths of the porous, atomically-thick Co_3O_4 sheets. In addition, the 30% pore occupancy facilitated easy electrolyte infiltration and ensured a large contact area with the electrolyte, thus enlarging the reaction space. As a result, the atomically-thick Co_3O_4 porous sheets yielded an electrocatalytic current up to 341.7 mA cm^{-2} at 1.0 V *vs.* Ag/AgCl, roughly 50- and 30-times larger than that of the bulk counterpart and commercial 20 wt% Pt/C. As far as we know, such an electrocatalytic reaction current of 341.7 mA cm^{-2} is significantly higher than that of most existing reports under similar conditions. Briefly, this work not only provides a facile and scalable strategy for fabricating atomically-thin porous sheets of non-layered compounds but also proves that the peculiar structures are outstanding platforms for optimizing water oxidation at the atomic level, holding great promise for triggering breakthroughs in the field of electrocatalysis.

Experimental section

Synthesis of ultrathin CoO sheets

In a typical procedure, 100 mg Co(acac)$_3$ was added into a mixed solution of 20 mL ethylene glycol and 4 mL distilled water, followed by vigorous stirring for 30 min. Then the mixture was transferred into a 50 mL Teflon-lined autoclave, sealed and heated at 190 °C for 48 h. The system was then allowed to cool to room temperature naturally, the final product was collected by centrifuging the mixture, washed with ethanol and water many times, and then dried under vacuum overnight for further characterization.

Synthesis of porous Co_3O_4 ultrathin sheets

In a typical procedure, the as-obtained ultrathin CoO sheets were directly heated at 400 °C for 5 min in air and then cooled to room temperature. The obtained powders were collected for further characterization.

Synthesis of bulk Co_3O_4

In a typical procedure, 1 g Co(NO$_3$)$_2$·6H$_2$O was heated at 900 °C for 24 h in air and then cooled to room temperature. The obtained powders were collected for further characterization.

Characterization

Transmission electron microscopy (TEM) images and high-resolution TEM image were performed by using a JEOL-2010 TEM with an acceleration voltage of 200 kV. The field emission scanning electron microscopy (FE-SEM) images were obtained using an FEI Sirion-200 SEM. XRD patterns were recorded using a Philips X'Pert Pro Super diffractometer with Cu Kα radiation (λ = 1.54178 Å). X-ray photoelectron spectra (XPS) were acquired using an ESCALAB MKII with Mg Kα ($h\nu$ = 1253.6 eV) as the excitation source. The binding energies obtained in the XPS spectral analysis were corrected for specimen charging by referencing C 1s to 284.5 eV. Atomic force microscopy (AFM) studies in the present work were performed by means of a Veeco DI Nano-scope MultiMode V system. Raman spectra were collected using a Renishaw RM 3000 Micro-Raman system. The IR spectra were measured using a NICOLET FT-IR spectrometer, using pressed KBr tablets. Thermal gravimetric analysis (TGA) of the as-synthesized samples was carried out on a Shimadzu TA-50 thermal analyzer at a heating rate of 10 °C min^{-1} from room temperature to 800 °C.

Electrochemical measurements

Electrochemical measurements were carried out in a three-electrode system at an electrochemical station (CHI660B). Typically, 5 mg of sample and 30 μL of Nafion solution (5 wt%) were dispersed in 1 mL water–ethanol solution with a volume ratio of 3 : 1 by sonicating for 1 h to form a homogeneous ink. Then, 5 μL of the dispersion (containing 24 μg of catalyst) was loaded onto a glassy carbon electrode of 3 mm diameter (loading ∼0.34 mg cm^{-2}). Linear sweep voltammetry at a scan rate of 5 mV s^{-1} was conducted in 1.0 M KOH. The KOH electrolyte was purged with nitrogen for 30 min prior to the measurement. The glassy carbon electrode served as the working electrode. The counter and the reference electrodes were a platinum gauze and the Ag/AgCl reference electrode, respectively.

Calculation details

The first-principles calculations were performed by employing the Vienna *ab initio* simulation package[20] using a generalized gradient approximation augmented by a Hubbard U term

(GGA+U) with PBE functional.[21] The energy cutoff is set to 600 eV, and the atomic positions are allowed to relax until the energy and force are less than 10^{-4} eV and 5×10^{-3} eV Å^{-1}, respectively. The on-site repulsion is treated within Dudarev's approach, where the on-site Coulomb repulsion (Hubbard U) and the atomic-orbital intra-exchange energy (Hund's parameter J) are simplified to one parameter U_{eff} ($U_{eff} = U - J = 2.0$ eV). The porous Co_3O_4 atomically-thin sheets were simulated by periodically repeating the CoO layers along the [001] direction of the unit cell. Each sheet model has the thickness of half a unit cell along the [001] direction and is separated by a vacuum region of 15 Å. An elliptical pore area by removing partial Co and O atoms on the ultrathin sheet was used to simulate the pore. The comparison calculations for bulk Co_3O_4 were performed within supercells constructed from a standard unit cell of the Co_3O_4 lattice.

Acknowledgements

Notes and references

1 (a) Y. F. Sun, H. Cheng, S. Gao, Z. H. Sun, Q. H. Liu, Q. Liu, F. C. Lei, T. Yao, J. F. He, S. Q. Wei and Y. Xie, *Angew. Chem., Int. Ed.*, 2012, **51**, 8727; (b) S. Y. Reece, J. A. Hamel, K. Sung, T. D. Jarvi, A. J. Esswein, J. J. H. Pijpers and D. G. Nocera, *Science*, 2011, **334**, 645.

2 (a) J. Rosen, G. S. Hutchings and F. Jiao, *J. Am. Chem. Soc.*, 2013, **135**, 4516; (b) A. Kudo and Y. Miseki, *Chem. Soc. Rev.*, 2009, **38**, 253.

3 (a) Y. Zhao, R. Nakamura, K. Kamiya, S. Nakanishi and K. Hashimoto, *Nat. Commun.*, 2013, **4**, 2390; (b) M. R. Gao, Y. F. Xu, J. Jiang, Y. R. Zheng and S. H. Yu, *J. Am. Chem. Soc.*, 2012, **134**, 2930.

4 (a) M. G. Walter, E. L. Warren, J. R. Mckone, S. W. Boettcher, Q. Mi, E. A. Santori and N. S. Lewis, *Chem. Rev.*, 2010, **110**, 6446; (b) J. Wang, H. X. Zhong, Y. L. Qin and X. B. Zhang, *Angew. Chem., Int. Ed.*, 2013, **52**, 5248.

5 (a) M. M. Najafpour, T. Ehrenberg, M. Wiechen and P. Kurz, *Angew. Chem., Int. Ed.*, 2010, **49**, 2233; (b) N. S. McCool, D. M. Robinson, J. E. Sheats and G. C. Dismukes, *J. Am. Chem. Soc.*, 2011, **133**, 11446.

6 (a) F. Jiao and H. Frei, *Angew. Chem., Int. Ed.*, 2009, **48**, 1841; (b) J. Wu, Y. Xue, X. Yan, W. S. Yan, Q. M. Cheng and Y. Xie, *Nano Res.*, 2012, **5**, 521; (c) F. Jiao and H. Frei, *Energy Environ. Sci.*, 2010, **3**, 1018; (d) C. Z. Yuan, L. Yang, L. R. Hou, L. F. Shen, X. G. Zhang and X. W. Lou, *Energy Environ. Sci.*, 2012, **5**, 7883.

7 (a) Y. Xu, R. Yi, B. Yuan, X. F. Wu, M. Dunwell, Q. L. Lin, L. Fei, S. G. Deng, P. Andersen, D. H. Wang and H. M. Luo, *J. Phys. Chem. Lett.*, 2012, **3**, 309; (b) Y. Q. Fan, H. B. Shao,

J. M. Wang, L. Liu, J. Q. Zhang and C. N. Cao, *Chem. Commun.*, 2011, **47**, 3469.

8 (a) M. W. Kanan and D. G. Nocera, *Science*, 2008, **321**, 1072; (b) R. D. L. Smith, M. S. Prévot, R. D. Fagan, Z. P. Zhang, P. A. Sedach, M. K. J. Siu, S. Trudel and C. P. Berlinguette, *Science*, 2013, **340**, 60; (c) W. D. Chemelewski, H. C. Lee, J. F. Lin, A. J. Bard and C. B. Mullins, *J. Am. Chem. Soc.*, 2014, **136**, 2843; (d) R. D. L. Smith, M. S. Prévot, R. D. Fagan, S. Trudel and C. P. Berlinguette, *J. Am. Chem. Soc.*, 2013, **135**, 11580; (e) J. D. Blakmore, N. D. Schley, G. W. Olack, C. D. Incarvito, G. W. Brudvig and R. H. Crabtree, *Chem. Sci.*, 2011, **2**, 94; (f) M. Dincǎ, Y. Surendranath and D. G. Nocera, *Proc. Natl. Acad. Sci. U. S. A.*, 2010, **107**, 10337; (g) I. Zaharieva, P. Chernev, M. Risch, K. Klingan, M. Kohlhoff, A. Fischer and H. Dau, *Energy Environ. Sci.*, 2012, **5**, 7081.

9 (a) Y. F. Sun, Z. H. Sun, S. Gao, H. Cheng, Q. H. Liu, J. Y. Piao, T. Yao, C. Z. Wu, S. L. Hu, S. Q. Wei and Y. Xie, *Nat. Commun.*, 2012, **3**, 1057; (b) J. B. Zhu, L. F. Bai, Y. F. Sun, X. D. Zhang, Q. Y. Li, B. X. Cao, W. S. Yan and Y. Xie, *Nanoscale*, 2013, **5**, 5241.

10 Y. F. Sun, H. Cheng, S. Gao, Q. H. Liu, Z. H. Sun, C. Xiao, C. Z. Wu, S. Q. Wei and Y. Xie, *J. Am. Chem. Soc.*, 2012, **134**, 20294.

11 (a) B. Radisavljevic, A. Radenovic, J. Brivio, V. Giacometti and A. Kis, *Nat. Nanotechnol.*, 2011, **6**, 147; (b) Y. F. Sun, S. Gao and Y. Xie, *Chem. Soc. Rev.*, 2014, **43**, 530.

12 (a) S. Ithurria, M. D. Tessier, B. Mahler, R. P. S. M. Lobo, B. Duberttret and A. L. Efros, *Nat. Mater.*, 2011, **10**, 936; (b) C. Schliehe, B. H. Juarez, M. Pelletier, S. Jander, D. Greshnykh, M. Nagel, A. Meyer, S. Foerster, A. Kornowski, C. Klinke and H. Weller, *Science*, 2012, **329**, 550.

13 (a) Y. Shi, Y. Wan and D. Zhao, *Chem. Soc. Rev.*, 2011, **40**, 3854; (b) J. S. Chen, T. Zhu, X. H. Yang, H. G. Yang and X. W. Lou, *J. Am. Chem. Soc.*, 2010, **132**, 13162.

14 (a) Z. L. Zhang, Z. Y. Tang, N. A. Kotov and S. C. Glotzer, *Nano Lett.*, 2007, **7**, 1670; (b) Z. Y. Tang, Z. L. Zhang, Y. Wang, S. C. Glotzer and N. A. Kotov, *Science*, 2006, **314**, 274.

15 C. Z. Yuan, L. Yang, L. R. Hou, J. Y. Li, Y. X. Sun, X. G. Zhang, L. F. Shen, X. J. Lu, S. L. Xiong and X. W. Lou, *Adv. Funct. Mater.*, 2012, **22**, 2560.

16 (a) Y. F. Sun, Z. H. Sun, S. Gao, H. Cheng, Q. H. Liu, F. C. Lei, S. Q. Wei and Y. Xie, *Adv. Energy Mater.*, 2014, **4**, 1300611; (b) Y. F. Sun, J. B. Zhu, L. F. Bai, Q. Y. Li, X. Zhang, W. Tong and Y. Xie, *Inorg. Chem. Front.*, 2014, **1**, 58.

17 (a) Y. Y. Liang, Y. G. Li, H. L. Wang, J. G. Zhou, J. Wang, T. Regier and H. J. Dai, *Nat. Mater.*, 2011, **10**, 780; (b) Y. Y. Liang, H. L. Wang, J. G. Zhou, Y. G. Li, J. Wang, T. Regier and H. J. Dai, *J. Am. Chem. Soc.*, 2012, **134**, 3517; (c) A. J. Esswein, M. J. McMudo, P. N. Ross, A. T. Bell and T. D. Tilley, *J. Phys. Chem. C*, 2009, **113**, 15068; (d) H. Tüysüz, Y. J. Hwang, S. B. Khan, A. M. Asin and P. D. Yang, *Nano Res.*, 2013, **6**, 47; (e) N. H. Chou, P. N. Ross, A. T. Bell and T. D. Tilley, *ChemSusChem*, 2011, **4**, 1566.

18 (*a*) E. Rios, P. Chartier and J. L. Gautier, *Solid State Sci.*, 1999, **1**, 267; (*b*) M. Hamdani, R. N. Singh and P. Chartier, *Int. J. Electrochem. Sci.*, 2010, **5**, 556.

19 (*a*) M. Bajdich, M. García-Mota, A. Vojvodic, J. K. Nørskov and A. T. Bell, *J. Am. Chem. Soc.*, 2013, **135**, 13521; (*b*) Y. F. Sun, S. S. Jiang, W. T. Bi, C. Z. Wu and Y. Xie, *J. Power Sources*, 2011, **196**, 8644.

20 (*a*) G. Kresse and D. Joubert, *Phys. Rev. B: Condens. Matter Mater. Phys.*, 1999, **59**, 1578; (*b*) G. Kresse and J. Furthmuller, *Phys. Rev. B: Condens. Matter Mater. Phys.*, 1996, **54**, 11169.

21 P. Perdew, K. Burke and M. Ernzerhof, *Phys. Rev. Lett.*, 1996, **77**, 3865.